Available online at www.sciencedirect.com
ScienceDirect
Journal of Solid State Chemistry 180 (2007) 619–627
JOURNAL OF SOLID STATE CHEMISTRY
www.elsevier.com/locate/jssc

Structural, spectroscopic and photoluminescence studies of $LiEu(WO_4)_{2-x}(MoO_4)_x$ as a near-UV convertible phosphor

Chuang-Hung Chiu[a], Ming-Fang Wang[b], Chi-Shen Lee[b], Teng-Ming Chen[a,*]

[a]*Phosphors Research Laboratory, Department of Applied Chemistry, National Chiao Tung University, Hsinchu 30010, Taiwan*
[b]*Applied Inorganic Solid-State Laboratory, Department of Applied Chemistry, National Chiao Tung University, Hsinchu 30010, Taiwan*

Received 25 July 2006; received in revised form 30 October 2006; accepted 13 November 2006
Available online 17 November 2006

Abstract

A series of lithium europium double tungsto-molybdate phosphors $LiEu(WO_4)_{2-x}(MoO_4)_x$ ($x = 0$, 0.4, 0.8, 1.2, 1.6, 2.0) have been synthesized by solid-state reactions and their crystal structure, optical and luminescent properties were studied. As the molybdate content increases, the intensity of the $^5D_0 \rightarrow {}^7F_2$ emission of Eu^{3+} activated at wavelength of 396 nm was found to increase and reach a maximum when the relative ratio of Mo/W is 2:0. These changes were found to be accompanied with the changes in the spectral feature, which can be attributed to the crystal field splitting of the $^5D_0 \rightarrow {}^7F_2$ transition. As the molybdate content increases the emission intensity of the 615 nm peak also increases. The intense red-emission of the tungstomolybdate phosphors under near-UV excitation suggests them to be potential candidate for white light generation by using near-UV LEDs. In this study the effect of chemical compositions and crystal structure on the photoluminescent properties of $LiEu(WO_4)_{2-x}(MoO_4)_x$ is investigated and discussed.

Keywords: Phosphors; $LiEu(WO_4)_{2-x}(MoO_4)_x$; Photoluminescence; LED

1. Introduction

White light-emitting diodes (LEDs), the so-called next-generation solid-state lighting (SSL), offer benefits in accordance with stability, energy-saving, perpetuation and safety, and consequently, are receiving much attention. The availability of white LEDs is expected to open up a great number of exciting new application fields: white light sources to replace traditional incandescent and fluorescent lamps, backlights for portable electronics, medical, and architecture lightings, etc. [1]. The first LED produced in 1996, an excellent method using a blue LED chip in combination with a phosphor that exhibits yellow emission under blue excitation was proposed [2]. The yellow phosphor is a Ce^{3+}-activated yttrium aluminum garnet, $(Y,Gd)_3(Al,Ga)_5O_{12}:Ce^{3+}$.[3] Nowadays, the products of white LEDs have a general color rendering index (Ra) of ~85, which is enough for universal illumination [4]. However, these white LEDs are not applicable for certain medical applications and architectural lighting purposes due to the deficient red emission. In order to achieve high luminous output, the emission band should have full-width at half-maximum (FWHM) as small as possible.[5] The red light-emitting phosphors used for improving Ra and tuning color temperature of the white-light LEDs are still limited commercially to sulfide-based materials such as $CaS:Eu^{2+}$, $SrY_2S_4:Eu^{2+}$, and ZnCdS:Cu,Al [6,7]. However, there are certain disadvantages to using those sulfide-based materials, such as chemical instability, high FWHM, and low efficiency [8].

Therefore, the search for a stable, inorganic rare earth-based red phosphor with high absorption in the near-UV/blue spectral region is therefore an attractive and challenging research task. The potassium lanthanide double tungstates and double molybdates crystals were reported by Kaminskii to be efficient luminescent hosts for rare earth and transition metal ions [9]. The phonon properties of $KEu(MoO_4)_2$ and $KEu(WO_4)_2$ were described by Macalik [10]. Hanuza et al. [11] reported the spectroscopic properties of Eu^{3+} ion in $KEu(MoO_4)_2$ crystal (as monoclinic $P2_1/c$ with $Z = 12$) and the same group of

*Corresponding author. Fax: +886 3 572 3764.
E-mail address: tmchen@mail.nctu.edu.tw (T.-M. Chen).

0022-4596/$ - see front matter © 2006 Elsevier Inc. All rights reserved.
doi:10.1016/j.jssc.2006.11.015

researchers also reported the electronic absorption and emission spectra of Eu^{3+} in $KEu(WO_4)_2$ [12] (crystallized in the monoclinic space group C_{2h}^6 with four molecules per unit-cell). In addition, Macalik et al. [13] detailed the optical and magnetic properties of double rare-earth molybdates and tungstates with composition of $MR(XO_4)_2$, where $M = Cs$, K, Rb, $R =$ rare earth, and $X = Mo$, W, which are of interest because these crystals display a number of fascinating peculiar features associated with a low symmetry of the crystal lattice by Khatsko [14].

The luminescence spectra of scheelite-type $Li(Y_{1-x}Eu_x)(MoO_4)_2$ ($x = 0.0005$, 0.001, 0.01, 0.05, 0.1, 0.5, 1) solid solutions were investigated by Zaushitsyn et al. [15] using laser excitation at 337.1 nm. According to the XRD data, $LiY(MoO_4)_2$ and $LiEu(MoO_4)_2$ form a continuous series of scheelite solid solutions (tetragonal symmetry, space group $I4_1/a$). The authors investigated the effect of Eu^{3+} concentration on the luminescence behavior of the solid solutions. The strongest integrated emission intensity was observed in $LiY_{0.5}Eu_{0.5}(MoO_4)_2$ and the substitution of Eu^{3+} for Y^{3+} has no effect on the site symmetry of the emission centers involved. Furthermore, the luminescence of composition-optimized double molybdates ($Li_{0.333}Na_{0.334}K_{0.333}$) $Eu(MoO_4)_2$ (LNKEM), showing strong luminescent intensity was reported by Wang et al. [16]. It is an excellent red-emitting LED phosphor due to its suitable particle size, high stability, fairly intense red-emission with its CIE chromaticity coordinates close to those of NTSC red with CIE coordinates (0.67, 0.33) than that of $Y_2O_2S{:}0.05Eu^{3+}$. Very recently, Sivakumar and Varadaraju [8] reported an intense near-UV and blue- (i.e., 394 and 465 nm) convertible red-emitting tungstomolybdate phosphor with composition of $AgGd_{0.95}Eu_{0.05}(WO_4)_{2-x}(MoO_4)_x$ ($x = 0-2$) and investigated its photoluminescence (PL) and chromaticity properties.

Motivated by the above-stated investigations and the attempts to develop phosphors excitable by near-UV and/or blue radiation for the applications of white-light LED, we have investigated and reported herein the results of crystal structure refinements, PL and color chromaticity properties of $LiEu(WO_4)_{2-x}(MoO_4)_x$ ($0 \leqslant x \leqslant 2.0$) phosphors.

2. Experimental section

The samples of $LiEu(WO_4)_{2-x}(MoO_4)_x$ ($x = 0$, 0.4, 0.8, 1.2, 1.6, 2.0) phosphors were prepared by first ball-milling a reactant mixture consisting of stoichiometric amount of Li_2CO_3 (99.9%), Eu_2O_3 (99.99%), MoO_3 (99.9%) and WO_3 (99.9%) (all from Aldrich Chemicals, Milwaukee, WI, USA) by using a vibrational agate ball mill (Retsch model MM2000) for 20–30 min and then fired at 600–800 °C for 6 h

$$Li_2CO_3 + Eu_2O_3 + 2(2-x)WO_3 + 2xMoO_3 \rightarrow 2LiEu(WO_4)_{2-x}(MoO_4)_x + CO_2.$$

The products obtained were found to be polycrystalline and the X-ray diffraction (XRD) patterns were recorded using a Bruker D8 Advanced diffractometer equipped with Cu$K\alpha$ radiation ($\lambda = 1.5418$ Å) operating at 40 kV and 40 mA. XRD data for phase identification and structure refinements were collected in a 2θ range from 10° to 80° with a step interval of 0.02°/10 s and 0.01°/17 s, respectively. The powder diffraction data containing of 7000 reflections were subjected to processing and analysis using a computer software GSAS package (general structure analysis system), which is capable of handling such data simultaneously for performance of structure refinement [17–19]. The starting structure model of each sample came from $KEu(MoO_4)_2$ structure data base (ICSD Collection Code 6138) [20]. Refined structure parameters included overall scale factors, lattice parameters, and fractional coordinates. Absorption parameters and an extinction coefficient were also refined. Backgrounds were fitted using an analytical function with twenty four parameters, and peak shapes were fitted using exponential pseudo-Voigt functions. The Li/Eu sites have been allowed to vary in the refinement and the results are close to 50% Li + 50% Eu for both patterns. Therefore, the occupancies of Li/Eu sites were fixed at 50%/50% Eu to maintain the charge balance for both refinements. The isotropic atomic displacement parameters, U_{iso}, yielded unreasonable small or negative values during the refinements, which were fixed at 0.025 to all sites.

The measurements of PL and photoluminescence excitation (PLE) spectra were performed by using a Spex Fluorolog-3 spectrofluorometer (Instruments S.A., NJ, USA) equipped with a 450 W Xe light source and double excitation monochromators. The powder samples were compacted and excited under 45° incidence and the emitted fluorescence was detected by a Hamamatsu Photonics R928 type photomultiplier perpendicular to the excitation beam. The spectral response of the measurement system is calibrated automatically on start up. To eliminate the second-order emission of the source radiation, a cut-off filter was used in the measurements. For the comparison of PLE and PL intensity, the quantity of the phosphor samples has been normalized and measurement conditions (i.e., width of slit of the excitation and emission monochromators, the packing density of samples, the PMT detector sensitivity) were kept consistent from sample to sample in the measurements.

The diffuse reflectance (DR) spectra of the phosphor samples were measured with a Hitachi 3010 double-beam UV-VIS spectrometer (Hitachi Co., Tokyo, Japan) equipped with a $\varnothing$ 60 mm integrating sphere whose inner face was coated with $BaSO_4$ or Spectralon and α-Al_2O_3 was used as a standard in the measurements. The Commission International de I'Eclairage (CIE) chromaticity coordinates for all samples were determined by a Laiko DT-100 color analyzer equipped with a CCD detector (Laiko Co., Tokyo, Japan).

3. Results and discussion

3.1. Phase characterizations and X-ray structure analyses

Figs. 1(a) and (b) show the measured, calculated, and the difference between the calculated and observed XRD patterns of $LiEu(WO_4)_2$ and $LiEu(MoO_4)_2$, respectively. Both patterns are properly indexed and show no unidentified diffraction peaks from impurity. The XRD pattern of $LiEu(MoO_4)_2$ is similar to that of $LiEu(WO_4)_2$. Both $LiEu(WO_4)_2$ and $LiEu(MoO_4)_2$ with the modified $KEu(MoO_4)_2$ structure were found to crystallize in the triclinic crystal system with space group P-1 and with two molecular units per unit-cell [20]. The crystallographic refinement data, atomic positions, and interatomic distances for both compounds are summarized in Table 1 (also see Supporting Information, Tables S1 and S2).

Table 1
Crystallographic data for $LiEu(WO_4)_2$ and $LiEu(MoO_4)_2$ at room temperature

	$LiEu(WO_4)_2$	$LiEu(MoO_4)_2$
Structure	Triclinic	Triclinic
Space group	$P\bar{1}$	$P\bar{1}$
Lattice parameters	$a = 10.4287(3)$	$a = 10.4094(3)$
	$b = 5.2079(1)$	$b = 5.1989(2)$
	$c = 6.7350(2)$	$c = 6.7540(2)$
	$\alpha = 112.764(5)$	$\alpha = 112.686(3)$
	$\beta = 112.716(3)$	$\beta = 112.575(2)$
	$\gamma = 89.930(3)$	$\gamma = 90.043(4)$
Z	2	2
R_{wp} (%)	6.69	4.29
R_p (%)	4.68	3.26
R_F (%)	9.58	14.44
Volume of unit cell	306.372(2)	306.604(4)
$Density_{cal}$ (g/cm^3)	7.096	5.054
χ^2	2.028	1.279

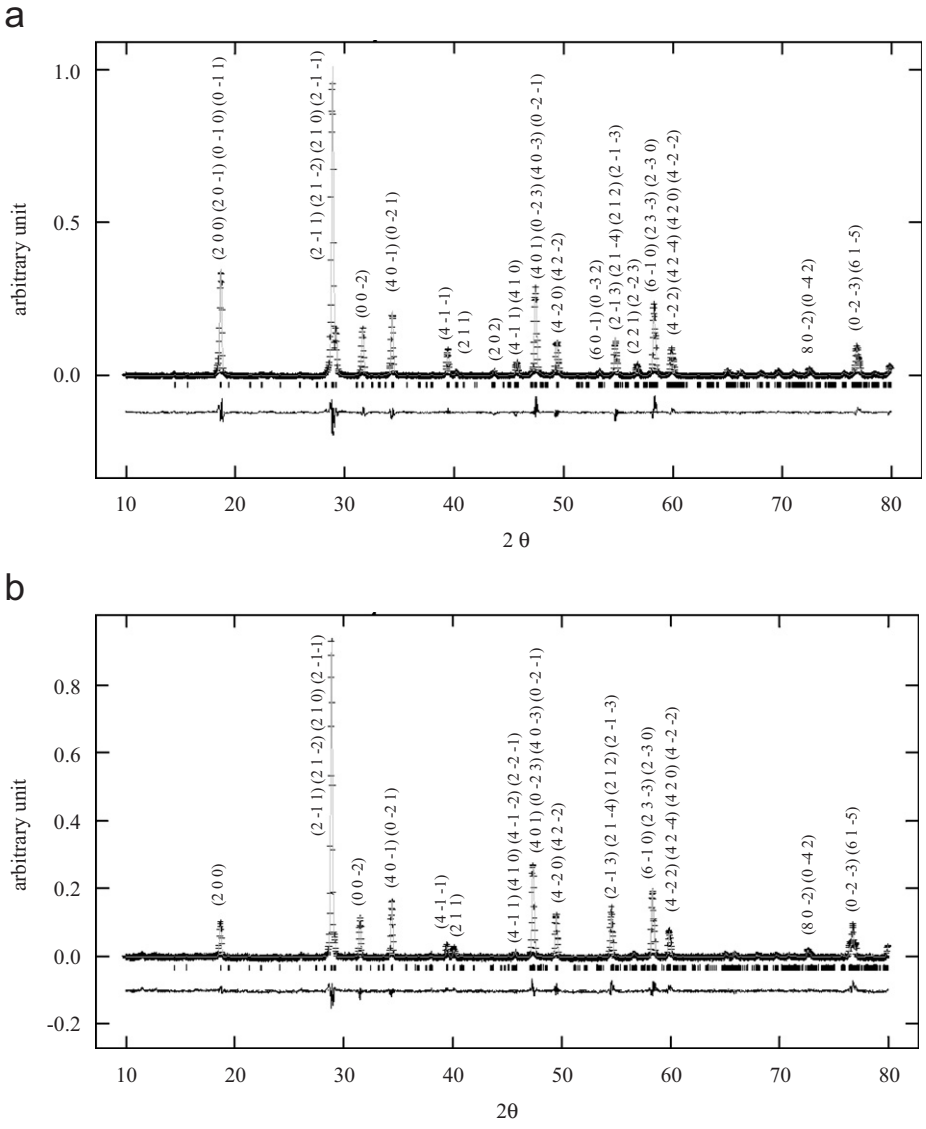

Fig. 1. Structure refinement patterns of $LiEu(MO_4)_2$ with M = (a) W and (b) Mo using X-ray powder diffraction data. Plus (+) marks represent the observed intensities, and the solid line defines the calculated pattern. The bottom curves represent difference (obs.−cal.) plots.

Crystal data of both compounds contain four sites for metal ions and eight sites for oxygen. Two metal site are mixed occupied by Eu^{3+} and Li^{+} ions in 1:1 ratio and the other two sites are occupied by M^{6+} (M = Mo, W) ions. Crystal structure of $LiEu(MO_4)_2$ (M = W, Mo) are shown in Fig. 2. Both $LiEu(WO_4)_2$ and $LiEu(MoO_4)_2$ are isostructure with $KEu(MoO_4)_2$, which are crystallized in the triclinic space group P-1 with $a = 10.4287(3)$ Å, $b = 5.2079(1)$ Å, $c = 6.7350(2)$ Å, $\alpha = 112.764(5)^\circ$, $\beta = 112.716(3)^\circ$, $\gamma = 89.930(3)^\circ$, $V = 306.372(2)$ Å^3, $Z = 2$ for $LiEu(WO_4)_2$, and $a = 10.4094(3)$ Å, $b = 5.1989(2)$ Å, $c = 6.7540(2)$ Å, $\alpha = 112.686(3)^\circ$, $\beta = 112.575(2)^\circ$, $\gamma = 90.043(4)^\circ$, $V = 306.604(4)$ Å^3, $Z = 2$ for $LiEu(MoO_4)_2$. The final weighted-profile R values (R_{wp}) were 6.69% and 4.29% for $LiEu(WO_4)_2$ and $LiEu(MoO_4)_2$, respectively. Both $LiEu(WO_4)_2$ and $LiEu(MoO_4)_2$ have four crystallographically distinct M sites which are occupied by lithium, europium and tungsten (or molybdenum) ions. The preliminary powder diffractogram of the polycrystalline single-phased $LiEu(MoO_4)_2$ gives prominent reflections between $2\theta = 10$–80° with a maximum at 28.92°, which corresponds to $d = 3.0842$ Å. The reflections match in intensity and position with the theoretical pattern of $KEu(MoO_4)_2$. Crystal structure of $LiEu(MO_4)_2$ (M = W and Mo) are depicted in Fig. 2(a) and (b). Black balls indicate mixed lithium and europium cations, gray ball are tungsten or molybdenum, and white balls indicate oxygen anions.

Shown in Fig. 3 is the comparison of XRD profiles for $LiEu(WO_4)_{2-x}(MoO_4)_x$ ($x = 0$, 0.2, 0.4, 1.2, 1.6, 2.0) phases as a function of doped Mo content (i.e., x). As the x value increases, the XRD profiles were found to be similar without showing discernable shifting, which can be rationalized by the almost identical ionic radius of Mo^{6+} and W^{6+}. We have also carried out an XRD cell parameters refinement based on 14–17 diffraction peaks obtained from the XRD profiles of $LiEu(WO_4)_{2-x}(MoO_4)_x$ using a triclinic crystal system and the results are summarized in Fig. 4. Our data show that as x increases the cell parameters a and b decreases, whereas c increases systematically, indicating that a solid solution is very likely to form between $LiEu(WO_4)_2$ and $LiEu(MoO_4)_2$ phases. Similar observation on solid solution formation has also been witnessed by Sivakumar and Varadaraju [8] in the $AgGd_{0.95}Eu_{0.05}(WO_4)_{2-x}(MoO_4)_x$ ($x = 0$–2) system.

As revealed by the SEM micrographs, we have found that the phosphor samples are well-defined aggregated crystalline grains below 10 μm with irregular shapes from the analysis of SEM images. These primary particles are

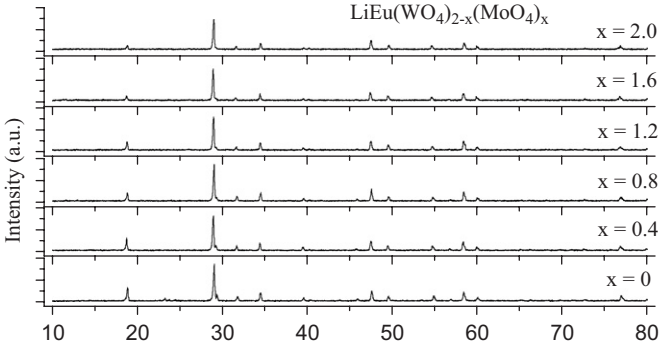

Fig. 3. Comparison of XRD profiles of $LiEu(WO_4)_{2-x}(MoO_4)_x$ phosphors with $x = 0$, 0.4, 0.8, 1.2, 1.6, and 2.0.

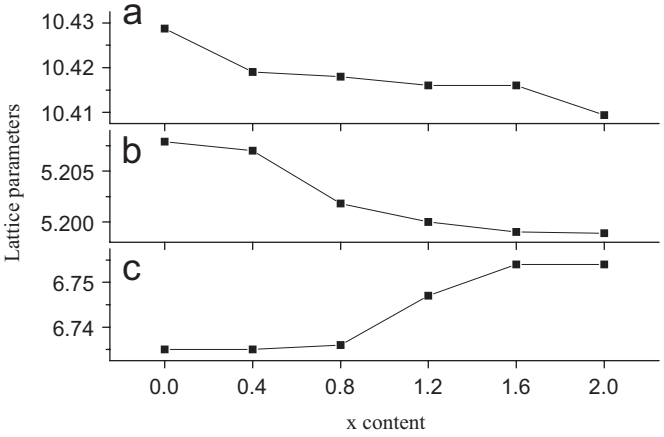

Fig. 4. Cell parameters as a function of x for $LiEu(WO_4)_{2-x}(MoO_4)_x$ phosphors.

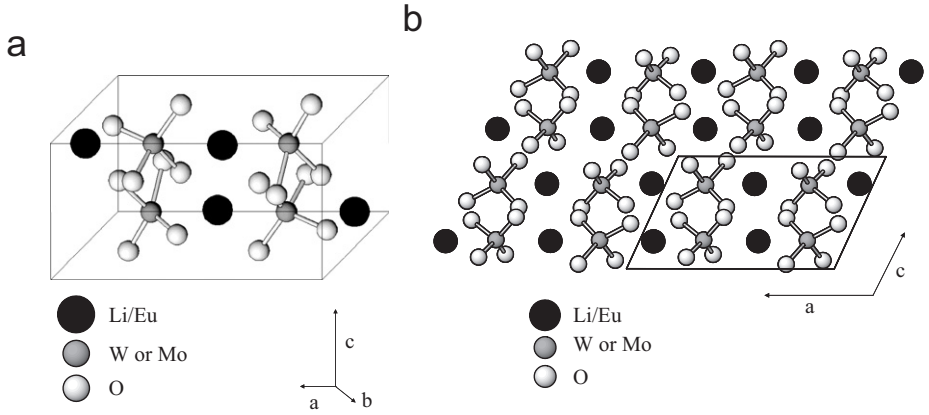

Fig. 2. Crystal structure of $LiEu(MO_4)_2$ (M = W and Mo): (a) unit cell view and (b) projection along b-axis.

both approximately 3–5 μm for $LiEu(MoO_4)_2$ and $LiEu(WO_4)_2$. The irregular grain morphology observed reveal the characteristics of the adopted solid-state method (see Supporting Information, Fig. S1).

3.2. Luminescent properties of $LiEu(WO_4)_{2-x}(MoO_4)_x$

Being monitored at 615 nm attributed to the $^5D_0 \rightarrow {}^7F_2$ emission of Eu^{3+} ions, the PLE spectra of six samples with selected compositions of $LiEu(WO_4)_{2-x}(MoO_4)_x$ ($x = 0$, 0.4, 0.8, 1.2, 1.6, 2.0) were shown in Fig. 5 for comparison, which were found to be similar to that of $(Li_{0.333}Na_{0.334}K_{0.333})Eu(MoO_4)_2$ reported by Wang et al. [16]. The intense broad band near 300 nm is assigned as the charge-transfer (CT) transition originated from oxygen to tungsten or molybdenum (i.e., ligand to metal CT) as discussed by Sivakumar and Varadaraju [8]. However, the CT band of Eu^{3+}–O^{2-} was not clearly observed in the excitation spectra, which could be due to possible overlap of the CT band with that of tungstate or molybdate group. In the range from 350 to 550 nm, all samples show characteristic intra-configurational 4*f*–4*f* emissive transitions of Eu^{3+}: sharp $^7F_0 \rightarrow {}^5L_6$ transition for 394 nm, $^7F_0 \rightarrow {}^5D_2$ transition for 465 nm, and the $^7F_1 \rightarrow {}^5D_1$ transition for 535 nm. As compared with the CT band, remarkable changes were observed in the intensity of characteristic absorptions of Eu^{3+} ion in the PLE spectra shown in Fig. 5, and the maximum absorption of Eu^{3+} $^7F_0 \rightarrow {}^5L_6$ peak becomes stronger with increasing molybdenum content. A 3-D spectral representation at the lower right of Fig. 5 shows the expanded PLE spectra in the spectral range 370–410 nm for comparison in detail.

Fig. 6 displays the composition-dependent PL spectra of $LiEu(WO_4)_{2-x}(MoO_4)_x$ ($x = 0$, 0.4, 0.8, 1.2, 1.6, 2.0) under 394 nm near-UV excitation. The spectra essentially consist of sharp lines with wavelength ranging from 580 to 720 nm, which are associated with the $^5D_0 \rightarrow {}^7F_J$ ($J = 1$, 2, 3, 4) transitions from the excited levels of Eu^{3+} to the ground state, although no emission corresponding to tungstate or molybdate is observed. However, the presence of an absorption band due to a tungstate or molybdate group in the excitation spectrum of Eu^{3+}, when monitored for Eu^{3+} emission (615 nm), clearly suggests that the energy absorbed by the WO_4^{2-}/MoO_4^{2-} group is transferred to Eu^{3+} levels nonradiatively. That is to say the emission corresponding to Eu^{3+} ions has been observed under excitation of the CT band of either WO_4^{2-} or MoO_4^{2-} group. This process has been known as "host-sensitized"[21] energy transfer. However, the intensity of Eu^{3+} emission is weaker with CT band excitation when compared to that due to Eu^{3+} excitation [8]. This reveals that the energy transfer from the WO_4^{2-}/MoO_4^{2-} group to Eu^{3+} is not efficient. The presence of multiplets in the emission spectra are attributed to the $(2J+1)$ Stark components of *J*-degeneracy splitting. The $^5D_0$ is the unsplitted singlet band, simplifying in a significant way the application of the group theory and of electronic transition selection rules. The electric–dipole allowed transition would be dominant when Eu^{3+} occupied the lattice site of noncentrosymmetric environment in the scheelite phases

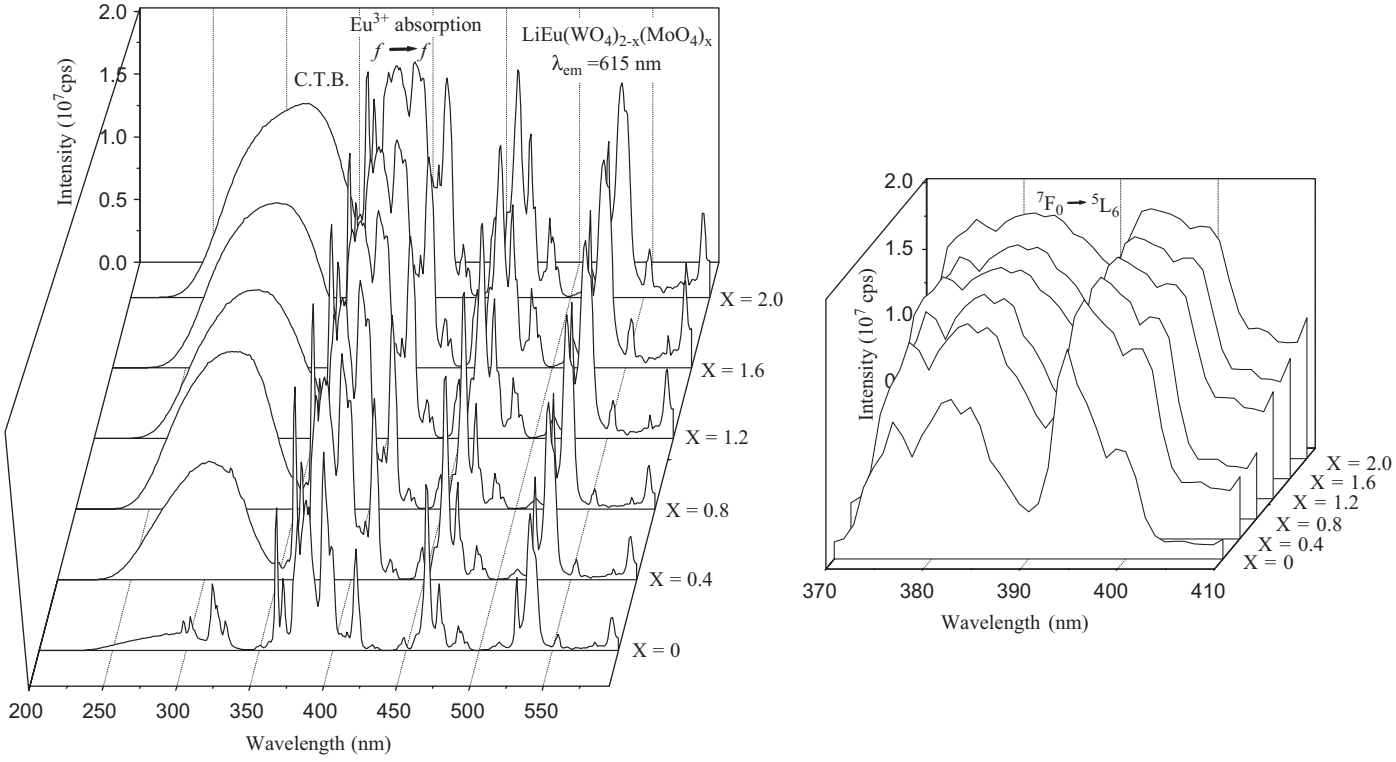

Fig. 5. PLE spectra monitored at 615 nm for $LiEu(WO_4)_{2-x}(MoO_4)_x$ phosphors with $x =$ (a) 0, (b) 0.4, (c) 0.8, (d) 1.2, (e) 1.6 and (f) 2.0.

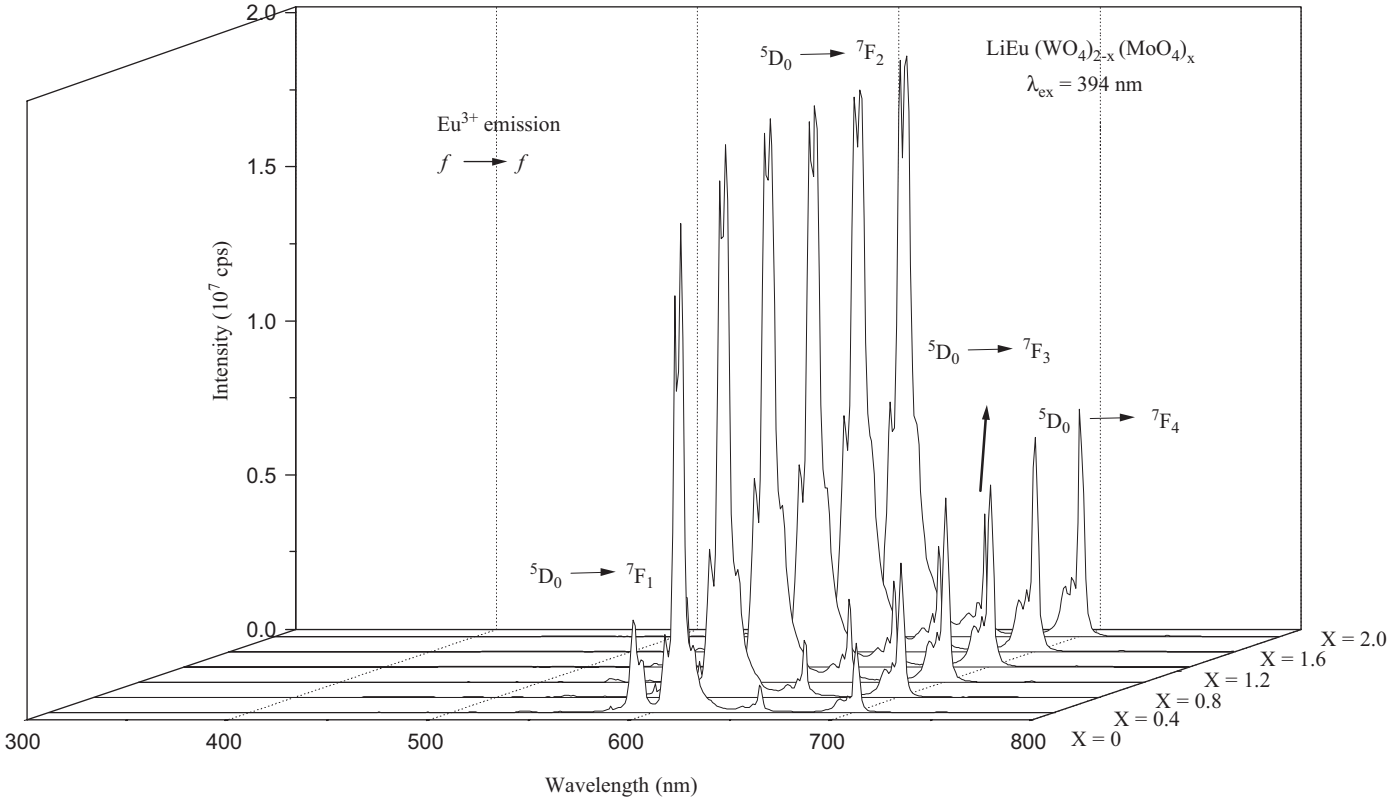

Fig. 6. PL spectra of $LiEu(WO_4)_{2-x}(MoO_4)_x$ ($x = 0$, 0.4, 0.8, 1.2, 1.6, 2.0) under 394 nm near-UV excitation.

[5]. For this reason, the intensity of $^5D_0 \rightarrow {}^7F_{2,4}$ (electric–dipole transition) was found to be much stronger than that of $^5D_0 \rightarrow {}^7F_{1,3}$ (magnetic–dipole transition). The major emission of $LiEu(WO_4)_{2-x}(MoO_4)_x$ was found at 615 nm ($^5D_0 \rightarrow {}^7F_2$), which corresponds to red emission. Other transitions of Eu^{3+} from the ^5D_J excited levels to ^7F_J ground states, for instance, $^5D_0 \rightarrow {}^7F_J$ is located at 570–720 nm and the $^5D_1 \rightarrow {}^7F_J$ transitions located at 520–570 nm are both very weak, and, therefore, the more saturated CIE chromaticity benefited greatly by the reasoning.

When the molybdenum content is increased, the lithium europium double tungsto-molybdate shows stronger red emission at 615 nm by exciting at near-UV wavelength of 394 nm. As indicated in Fig. 6, the intensity of $^5D_0 \rightarrow {}^7F_2$ transition was found to increase with the increasing doped Mo content and the I–λ curve reaches a maximum when the relative ratio of Mo/W is 2:0 as indicated in Table 2. The reason for this observation may be due to the advent of ion pair interaction between Eu^{3+} ions, which is expected to be much stronger in molybdate than in tungstate crystal because of the differences in the Eu^{3+}–Eu^{3+} distance in molybdate (average distance: 3.86(6) Å) and in tungstate (average distance: 3.9(1) Å) phosphors. One of the possibilities is that the distance between two Eu^{3+} ions can affect the energy transfer between the two ions.

In addition, to investigate the effect of alkali cation doping we have made an attempt to substitute Li^+ in $LiEu(MoO_4)_2$ with isovalent Na^+ and K^+ to form phosphors with $MEu(MoO_4)_2$ compositions (M = Na, K). The PLE and PL spectra of selected compositions $MEu(MoO_4)_2$ (M = Li, Na, K) were shown in Figs. 7 and 8, respectively. The alkali cations of Li^+ ($1s^2$), Na^+ ($2s^22p^6$) and K^+ ($3s^23p^6$) have the valence electronic configurations of inert gases. With atomic number increases, the cationic radii increase in order of $Li^+ < Na^+ < K^+$. In Fig. 7, the excitation intensity of PLE spectra was found to decrease with increasing size of alkali cations as shown by the comparison summarized in Table 2. Similarly, a systematic trend in the variation of emission spectra of three phosphors has also been observed. In both $LiEu(MoO_4)_2$ and $NaEu(MoO_4)_2$ compounds, the

Table 2
Comparison of excitation ($^7F_0 \rightarrow {}^5L_6$) and emission ($^5D_0 \rightarrow {}^7F_2$) intensity of $LiEu(WO_4)_{2-x}(MoO_4)_x$ phosphors

Compositions	Intensity (10^7 cps)	
	λ_{em} = 615 nm	λ_{ex} = 394 nm
$LiEu(WO_4)_2$	1.582	1.215
$LiEu(WO_4)_{1.6}(MoO_4)_{0.4}$	1.803	1.612
$LiEu(WO_4)_{1.2}(MoO_4)_{0.8}$	1.817	1.742
$LiEu(WO_4)_{0.8}(MoO_4)_{1.2}$	1.820	1.746
$LiEu(WO_4)_{0.4}(MoO_4)_{1.6}$	1.824	1.794
$LiEu(MoO_4)_2$	1.885	1.889
$NaEu(MoO_4)_2$	1.864	1.885
$KEu(MoO_4)_2$	1.800	1.800

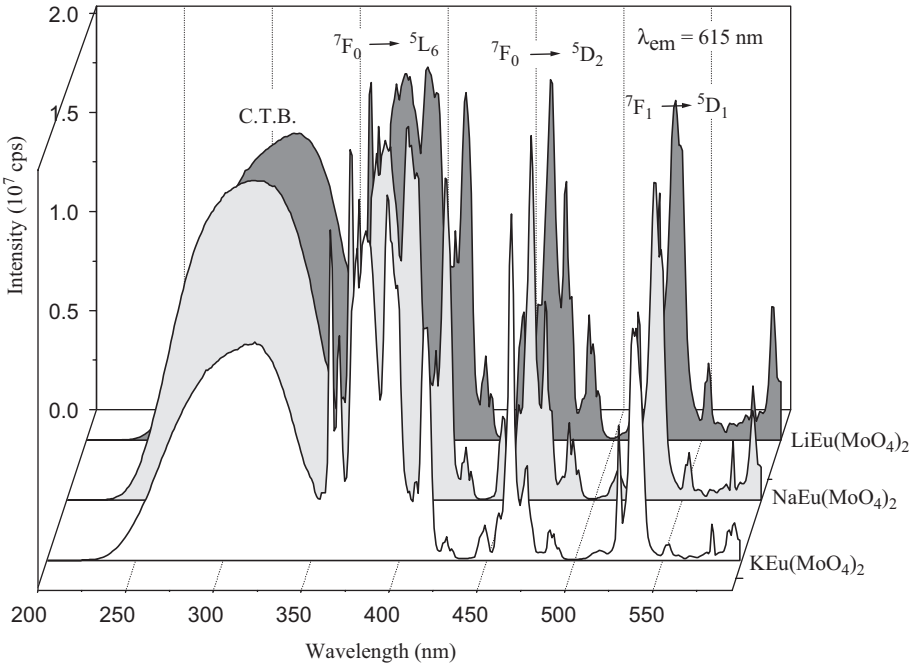

Fig. 7. Comparison of PLE spectra for phosphors of $M\mathrm{Eu(MoO_4)_2}$ (M = Li, Na, K).

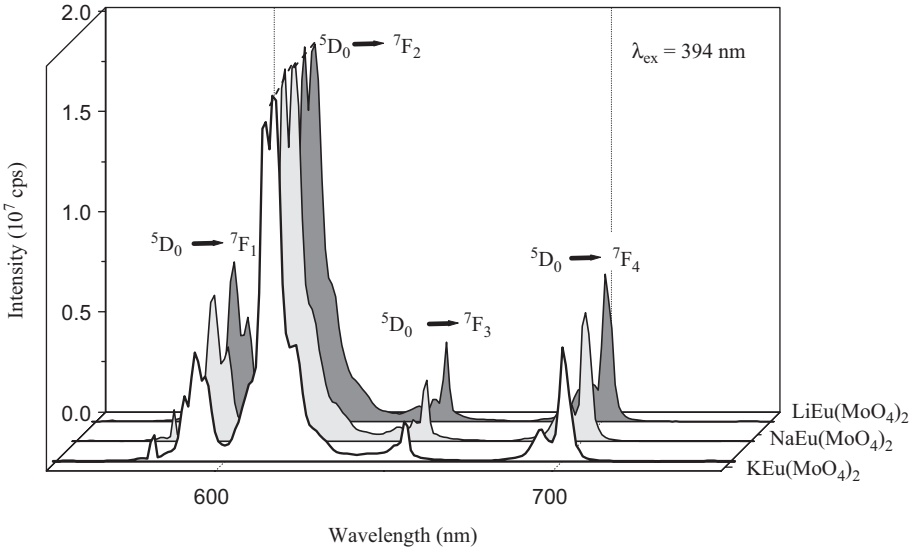

Fig. 8. Comparison of PL spectra for phosphors of $M\mathrm{Eu(MoO_4)_2}$ (M = Li, Na, K).

cations of Li^+ or Na^+ mixed with Eu^{3+} occupied the sites of space because the crystallographic data and refinements of $LiEu(MoO_4)_2$ indicate that two metal sites are mixedly occupied by Eu^{3+} and Li^+ ions in 1:1 ratio. Besides, the size of eight-coordinated Li^+(0.92 Å) or eight-coordinated Na^+(1.18 Å) is closer to that of Eu^{3+}(1.066 Å) than K^+(1.51 Å) [22]. In $LiEu(MoO_4)_2$ the Eu^{3+}–O^{2-} distance was found to be shortened, which could be attributed to the smaller size of Li^+ as compared to that of Na^+ or K^+. Consequently, the observed short Eu^{3+}–O^{2-} distance increases the probability for the exchange interaction to occur that resulted in the observed trend in the PL spectra. In $KEu(MoO_4)_2$ the cations of K^+ do not get mixed with Eu^{3+} that occupied the sites of space [20]. Since K^+ cation has the larger size than Li^+ and Na^+, thus, the Eu^{3+}–O^{2-} distance is longer. Under near-UV excitation at 394 nm the compound $KEu(MoO_4)_2$ displays the weakest luminescence intensity as compared to that of its analogs with M = Li and Na. Therefore, the observations described above rationalize why $LiEu(MoO_4)_2$ rather than $M\mathrm{Eu(MoO_4)_2}$ phosphors (M = Na, K) was chosen in our work.

3.3. DR spectra investigations of $LiEu(WO_4)_{2-x}(MoO_4)_x$

To investigate the optical properties of $LiEu(WO_4)_{2-x}(MoO_4)_x$ phosphors, we have also measured their

DR spectra as a function of x and the results are represented in Fig. 9. From the evolution of the reflection spectra, the observed absorption band centering at 300 nm tends to shift toward longer wavelength with increasing doped Mo content or x value. Furthermore, in almost all of the phosphors with varied x values, we have observed several absorptions at 300–350 (charge transfer transition O $2p \rightarrow$ Mo(W) ($4d(5d)$), 394 nm ($^7F_0 \rightarrow {}^5L_6$), 416 nm ($^7F_0 \rightarrow {}^5D_3$), 465 ($^7F_0 \rightarrow {}^5D_2$), and 535 nm ($^7F_1 \rightarrow {}^5D_1$), which were found to be consistent with those observed in the PLE spectra (shown in Fig. 5) and discussed previously in Section 3.2.

3.4. Investigations of chromaticity and luminance characteristics

In addition to the luminescence efficiency and brightness, the color chromaticity is also considered to be a critical parameter for evaluating the performance of LED phosphors from the aspect of application. The CIE color coordinates (x, y) and relative luminance of the our red-emitting phosphors investigated in this work are reported and compared against the commercial commodity $Y_2O_2S:Eu^{3+}$ (Kasei Optonix P22-RE3, the excellent excitation at $\lambda_{ex} = 342$ nm, PLE and PL illustrated in Fig. S2 in the Supporting Information) in Table 3. For the series of $LiEu(WO_4)_{2-x}(MoO_4)_x$ phosphors with different Mo/W ratios, the experimental CIE (x,y) coordinates indicate that as the concentration of Mo increases, the x-value increases while y-value decreases slightly and the chromaticity was found to shift away from red toward deep-red. In addition, we also found that with increasing doped Mo content the relative luminance increases from 0.8 ($x = 0$) to 1.4 ($x = 2.0$) monotonically. The CIE chromaticity coordinates were found to be (0.66, 0.33) for $LiEu(MoO_4)_2$ and it has reached the same level as the Kasei's commodity of $Y_2O_2S:Eu^{3+}$ (Catalog No. P22-RE3). It was also found that the CIE chromaticity coordinates of $LiEu(MoO_4)_2$ approach that (i.e., (0.67, 0.33)) of the NTSC red. Consequently, our investigation results indicate that $LiEu(WO_4)_{2-x}(MoO_4)_x$ is exceptionally attractive as a near-UV convertible phosphor as compared to the conventional $Y_2O_2S:Eu^{3+}$ in the application as a red-emitting phosphor for LEDs.

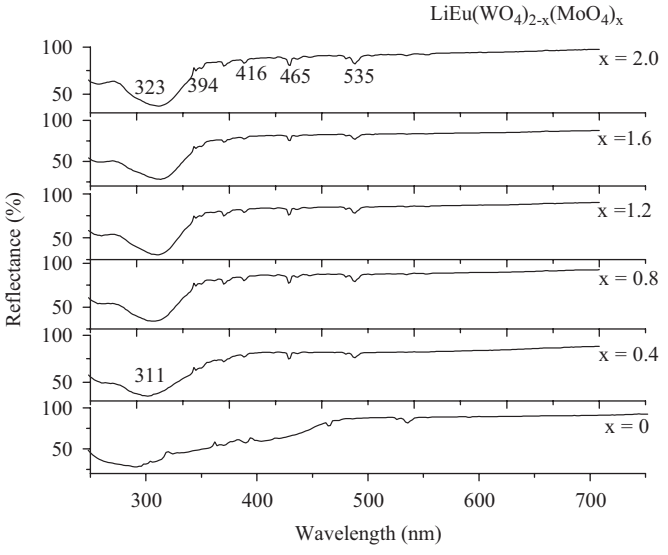

Fig. 9. Diffuse reflectance spectra of $LiEu(WO_4)_{2-x}(MoO_4)_x$ phosphors as a function of Mo content (x).

Table 3
Comparison of CIE chromaticity coordinates of phosphors investigated in the work

Phosphor compositions	CIE color coordinates (x, y)	Relative luminance (a.u.)
$LiEu(WO_4)_2$	(0.65, 0.35)	0.8
$LiEu(WO_4)_{1.6}(MoO_4)_{0.4}$	(0.65, 0.34)	0.9
$LiEu(WO_4)_{1.2}(MoO_4)_{0.8}$	(0.65, 0.34)	1.0
$LiEu(WO_4)_{0.8}(MoO_4)_{1.2}$	(0.65, 0.34)	1.1
$LiEu(WO_4)_{0.4}(MoO_4)_{1.6}$	(0.65, 0.34)	1.2
$LiEu(MoO_4)_2$	(0.66, 0.33)	1.4
$Y_2O_2S:Eu^{3+}$	(0.66, 0.33)	1.0

$\lambda_{ex} = 394$ nm for $LiEu(WO_4)_{2-x}(MoO_4)_x$; $\lambda_{ex} = 342$ nm for $Y_2O_2S:Eu^{3+}$.

4. Conclusions

We have successfully prepared a series of lithium europium double tungsto-molybdate $LiEu(WO_4)_{2-x}(MoO_4)_x$ ($x = 0$, 0.4, 0.8, 1.2, 1.6, 2.0) phosphors by solid-state reaction technique at high temperature. The synthesis, crystal structure, and luminescence properties under near-UV excitation of the double tungsto-molybdate phosphors have been investigated. Chromaticity characteristics and comparative luminance for the lithium europium double tungsto-molybdate phosphors have also been measured and compared with a commercial phosphor of $Y_2O_2S:Eu^{3+}$. This material has been found to exhibit efficient luminescence under excitation with irradiation of near ultraviolet radiation. In addition, it has also been established that lithium europium double tungsto-molybdate exhibits PL under excitation with blue-LED. For this reason, it has been attractive that $LiEu(WO_4)_{2-x}(MoO_4)_x$ can potential be a good red-emitting phosphor used in both near-UV and blue LEDs.

Acknowledgment

The research was supported by major funding from Institute of Optoelectronics of Industrial Technology Research Institute of Taiwan and, in part, from National Science Council of ROC under contract no. NSC94-2113-M-009-001.

Appendix A. Supplementary materials

Supplementary data associated with this article can be found in the online version at: doi:10.1016/j.jssc.2006.11.015.

References

[1] N. Hirosaki, R.J. Xie, K. Kimoto, Appl. Phys. Lett. 86 (2005) 211905.
[2] (a) S. Nakamura, T. Mukai, M. Sench, Appl. Phys. Lett. 64 (1994) 1687;
(b) S. Nakamura, S. Perton, G. Fasol, The Blue Laser Diode, Springer, Berlin, Germany, 1997, p. 230.
[3] K. Sakuma, K. Omichi, N. Kimura, M. Ohashi, Opt. Lett. 29 (2004) 2001.
[4] R. Xie, N. Hirosaki, K. Sakuma, Appl. Phys. Lett. 84 (2004) 5404.
[5] V. Sivakumar, U.V. Varadaraju, J. Electrochem. Soc. 153 (2006) H54.
[6] Y. Huh, J. Shim, Y. Kim, Y. Do, J. Electrochem. Soc. 150 (2003) H57.
[7] Y. Huh, J. Park, S. Kweon, J. Kim, J. Kim, Y.R. Do, Bull. Korean Chem. Soc. 25 (2004) 1585.
[8] V. Sivakumar, U.V. Varadaraju, J. Electrochem. Soc. 152 (2005) H168.
[9] A.A. Kaminskii, Laser Crystals. Their Physics and Properties, Springer, Berlin, Heidelberg, New York, 1981.
[10] L. Macalik, Pol. J. Chem. 69 (1995) 286.
[11] J. Hanuza, L. Macalik, B. Macalik, Acta Phys. Pol. A 84 (1993) 895.
[12] J. Hanuza, L. Macalik, B. Macalik, Acta Phys. Pol. A 84 (1993) 899.
[13] L. Macalik, B. Macalik, W. Strek, J. Legendziewicz, Eur. J. Solid Inorg. Chem. 33 (1996) 397.
[14] E.N. Khatsko,E-MRS Fall Meeting, 2005 Symposium B.
[15] A.V. Zaushitsyn, V.V. Mikhailin, A.Yu. Romanenko, E.G. Khaikina, O.M. Basovich, V.A. Morozov, B.I. Lazoryak, Inorg. Mater. 41 (2005) 766.
[16] Z. Wang, H. Liang, L. Zhou, H. Wu, M. Gong, Q. Su, Chem. Phys. Lett. 412 (2005) 313.
[17] C. Larson Allen, B. Von Dreele Robert, General Structure Analysis System (GSAS), Los Alamos National Laboratory Report LAUR, 2000, p. 86.
[18] B.H. Toby, EXPGUI, a graphical user interface for GSAS, J. Appl. Crystallogr. (2001) 210.
[19] C. Larson Allen, B. Von Dreele Robert, Los Alamos National Laboratory Report no. LAUR 86-748, 1987.
[20] R.F. Klevtsova, Kristallografiya 19 (1974) 89.
[21] G. Blasse, J. Chem. Phys. 45 (1969) 2356.
[22] R.D. Shannon, Acta Crystallogr. A 32 (1976) 751.